A Novel Route toward the Synthesis of High-Quality Large-Pore Periodic Mesoporous Organosilicas

Xiao Ying Bao,[†] X. S. Zhao,*[,†] Xu Li,[‡] Pai Ann Chia,[†] and Jun Li[‡]

Department of Chemical and Environmental Engineering, National University of Singapore, 10 Kent Ridge Crescent, Singapore 119620, and Institute of Materials Research and Engineering, 3 Research Link, Singapore 117602

Received: November 3, 2003; In Final Form: January 2, 2004

In this paper, we report a novel route to the synthesis of high-quality, large-pore periodic mesoporous organosilicas (PMOs) using triblock copolymer P123 as a template. The novelty lies in that highly ordered PMOs can only be synthesized at a limited range of low acid concentrations, which differs from traditional approach to the synthesis of similar materials including large-pore periodic mesoporous silicas (PMSs). The role that acid plays in the synthesis of high-quality PMOs and PMSs was critically examined, compared, and interpreted.

Introduction

Periodic mesoporous organosilicas (PMOs) synthesized by employing bridged silsesquioxanes $(RO)_3Si-R'-Si(OR)_3$ as silica sources are an emerging family of novel porous materials that combine the properties of organic and inorganic components in a composite material.[1−11] With uniformly distributed bridging functional groups (R′) in their frameworks, PMOs possess not only ordered mesopores but also various functional groups, offering a wider application potential over their pure inorganic counterparts. On the other hand, compared with nonporous or microporous organosilica materials,[12,13] the presence of highly developed pores of nanosize of PMOs affords both a higher density and a greater accessibility of the functional groups in applications such as catalysis,[11,14] adsorption,[15] and nanostructure templating.[16]

Since the pioneer reports of PMOs,[1−3] a great deal of study has been carried out in the synthesis of M41S[17] structures with small pore sizes. With regard to applications such as separation/purification of proteins where large pores are required, it is desirable to synthesize PMO materials with a pore size larger than that of M41S structures such as SBA-15,[18] a mesoporous material with pore size in the range of 6−30 nm. Although the synthesis of SBA-15 PMOs has been reported,[19−22] the materials are of poor quality. Improvements on structure order have been successful by using special synthetic techniques such as true liquid-crystal template,[23] and adding inorganic additives.[24] The employment of an additive brings about extra cost and additional parameters to be monitored. In addition, the added salts have been reported to be retained in the silica framework, having a deleterious effect on the framework hydrothermal stability.[25] The true liquid-templating approach presents challenges in controlling precursor diffusion in the liquid crystal phase and preventing precursor/liquid crystal phase separation.[26]

The present paper reports a novel pathway of synthesizing highly ordered, ethylene-bridged SBA-15 PMOs under controlled acidic conditions. By comparing the synthesis of PMOs with that of periodic mesoporous silicas (PMSs), we have, for the first time, identified the critical role of acid in the synthesis of SBA-15 type PMOs. Unlike SBA-15 PMSs, which can be synthesized over a wide range of acid concentrations,[18,27] the formation of highly ordered PMOs requires a much lower concentration of acid. In comparison with the previous studies,[19−24] which adopted the synthesis strategy of using high concentrations of acid that was reported in the synthesis of SBA-15 PMSs,[18] the method described here offers a simpler, more reproducible, and more cost-effective route to the preparation of high-quality PMO materials.

Experimental Section

Materials. 1,2-bis(trimethoxysilyl)ethane (BTMSE, 96%, Aldrich), 1,2-bis(triethoxysilyl)ethane (BTESE, 97%, Gelest), tetraethyl orthosilicate (TEOS, 98%, Fisher), triblock copolymer $EO_{20}PO_{70}EO_{20}$ (Pluronic P123, Aldrich), fuming hydrochloric acid (HCl, 37%, Merck), and absolute ethanol (99.98%, Merck) were used as received without further purification.

Synthesis. In a typical synthesis, 0.5 g of triblock copolymer $EO_{20}PO_{70}EO_{20}$ was combined with 7 mL of deionized water under stirring at 40 °C. A volume of 0.656 mL of BTMSE (or 0.955 mL of BTESE) was added to a mixture containing 7 mL of deionized water and 1.2 mL of 1.0 M HCl (prepared from 37% fuming HCl) at 40 °C. The P123−H_2O solution was then slowly added to the BTMSE (or BTESE)−H_2O−HCl mixture to obtain another mixture with a molar composition of Si/P123/HCl/H_2O = 1.00:0.0173:0.243:168. After further stirring for 24 h at 40 °C, the slurry was transferred into a polypropylene bottle and autoclaved at 100 °C for 120 h. The white solids were recovered by filtration, washed with deionized water and ethanol, and dried under ambient conditions.

To investigate the effect of acid, a series of samples were prepared following the above-described method by maintaining the amounts of Si, P123, and H_2O constant while varying the amount of HCl to obtain the molar ratios of HCl/H_2O in the range of 1.43×10^{-4} to 2.25×10^{-2}. The samples thus prepared are denoted MSE*y* (or ESE*y*), where MSE and ESE represent that the samples were prepared by using BTMSE and BTESE

* Author to whom correspondence should be addressed. E-mail: chezxs@nus.edu.sg.
[†] National University of Singapore.
[‡] Institute of Materials Research and Engineering.

10.1021/jp037342m CCC: $27.50
Published on Web 03/19/2004

TABLE 1: Molar Compositions for Synthesizing MSE*y*, ESE*y*, and OS*y* Materials

sample	SiO_2	P123	HCl	H_2O	HCl/H_2O
MSE1, ESE1, OS1	1.00	0.0173	0.024	168	1.43×10^{-4}
MSE2, ESE2, OS2	1.00	0.0173	0.048	168	2.86×10^{-4}
MSE3, ESE3, OS3	1.00	0.0173	0.119	168	7.08×10^{-4}
MSE4, ESE4, OS4	1.00	0.0173	0.243	168	1.45×10^{-3}
MSE5, ESE5, OS5	1.00	0.0173	0.490	168	2.92×10^{-3}
MSE6, ESE6, OS6	1.00	0.0173	1.064	168	6.33×10^{-3}
MSE7, ESE7, OS7	1.00	0.0173	3.773	168	2.25×10^{-2}

as the precursors, respectively; *y* is integers between 1 and 7, representing samples prepared at various HCl/H_2O molar ratios. Table 1 gives the details of sample names and molar compositions. No precipitation was observed for samples MSE1, ESE1, and ESE2 within 24 h of stirring. Therefore, samples MSE1 and ESE2 were prepared by further stirring under the same conditions for another 24 h before autoclaving.

For comparison purposes, PMS samples of SBA-15 structure were also synthesized by using TEOS as a silica source with the molar ratios of HCl/H_2O in the range of 1.43×10^{-4} to 2.25×10^{-2} (in the synthesis of the PMS materials, two moles of TEOS were considered to be equivalent to one mole of BTMSE or BTESE). The PMSs are designated as OS*y* with the same meaning of *y*.

Template Removal. Template P123 was removed by ethanol extraction[18] at 70 °C for 6 h.

Characterization. Small-angle X-ray scattering (SAXS) measurements were performed on a Bruker NanoStar at 40 kV and 35 mA with Cu Kα radiation. N_2 adsorption/desorption isotherms were measured on a Quantachrome NOVA 1200 system at 77 K. Samples were degassed at 323 K for 2 h before measurements.[28] Transmission electron microscope (TEM) images were obtained on a JEOL 2010 electron microscope operated at an acceleration voltage of 200 kV. Solid-state magic-angle spinning (MAS) nuclear magnetic resonance (NMR) spectra were collected on a Bruker DRX400 MHz FT-NMR spectrometer with a MAS speed of 8 kHz. Cross-polarization (CP) technique was used for both ^{13}C and ^{29}Si spectra, which were referenced to tetramethylsilane.

Results

The SAXS patterns of the MSE*y*, ESE*y*, and OS*y* materials are displayed in Figure 1. parts a, b, and c, respectively. Their unit cell parameters, *a*, are summarized in Table 2. Broad scattering peaks, suggesting disordered pore arrangement or small scattering domains, are seen on sample MSE7 (Figure 1a). Lowering the amount of acid improved the structural ordering, as indicated by the increase in the (100) peak intensity, the enhanced sharpness of the (100) peak, and the improved resolution of the higher order peaks. One intense peak at $2\theta \approx 0.80°$ and two or more weaker peaks at higher angles, which are characteristics of a 2D hexagonal structure with a *p6mm* symmetry,[18] are seen on samples MSE1−MSE6. The (100) peak intensity is the strongest for sample MSE3, while it was decreased when the HCl/H_2O ratios were higher or lower than 7.08×10^{-4}. The observed increase in the (100) peak intensity can be attributed to the improved long-range regularity. The decrease in (100) peak intensity at lower acid concentrations is most probably a consequence of the decreased level of organosilicate condensation, which lowers the framework-channel electron density contrast.

The SAXS patterns of samples ESE*y* (Figure 1b) essentially follow the similar trend to that of the MSE*y* materials. However, different from MSE*y* and ESE*y* materials, all OS*y* materials

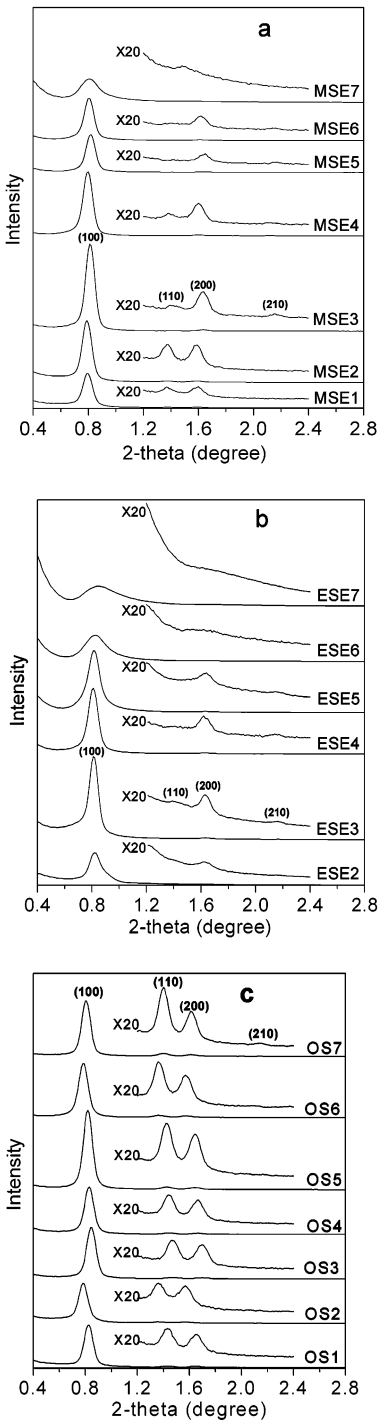

Figure 1. SAXS patterns of (a) MSE*y*, (b) ESE*y*, and (c) OS*y* materials synthesized at various HCl/H_2O ratios.

synthesized in this work exhibit highly ordered (*p6mm*) structures, as demonstrated by their well-resolved (100) peaks and the presence of (110) and (200) peaks (see Figure 1c). In contrast to SBA-15 PMOs, for which high (100) intensity is observed only at controlled acid concentrations, high (100) intensity is seen on OS*y* materials synthesized in the presence of high-concentration acid, which promoted the level of silicate condensation and hence the framework-channel electron density contrast.

Figure 1c also shows that for the OS*y* materials, the intensity ratio of peak (110) over peak (200), i.e., (110)/(200), increases continuously with increasing HCl/H_2O molar ratios. The opposite trend is observed for samples MSE*y* and ESE*y*, for which

TABLE 2: $d_{(100)}$ Spacings and Unit Cell Parameters Determined from SAXS Data[a]

sample	$d_{(100)}$ (nm)	a (nm)	sample	$d_{(100)}$ (nm)	a (nm)	sample	$d_{(100)}$ (nm)	a (nm)
MSE1[b,c]	11.2	12.9	ESE1[b]	N.A	N.A	OS1	10.6	12.3
MSE2	11.2	12.9	ESE2[b,c]	10.8	12.4	OS2	11.3	13.1
MSE3	10.9	12.6	ESE3	10.9	12.6	OS3	10.4	12.0
MSE4	11.0	12.8	ESE4	10.9	12.6	OS4	10.6	12.3
MSE5	10.8	12.4	ESE5	10.8	12.4	OS5	10.8	12.4
MSE6	11.0	12.8	ESE6	10.8	12.4	OS6	11.3	13.1
MSE7	10.9	12.6	ESE7	10.5	12.1	OS7	11.0	12.8

[a]The unit cell parameters, a, were determined from the interplanar spacings of the (100) planes using the formula of $a = 2d_{(100)}/\sqrt{3}$. [b] No precipitation was observed after 24 h of stirring. [c] Precipitation was observed after 48 h of stirring.

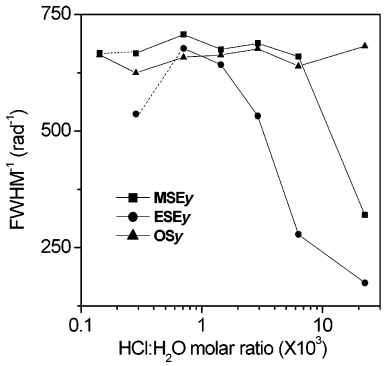

Figure 2. Reciprocal of fwhms of the (100) peaks as a function of the HCl/H_2O ratio for MSE*y*, ESE*y*, and OS*y* materials.

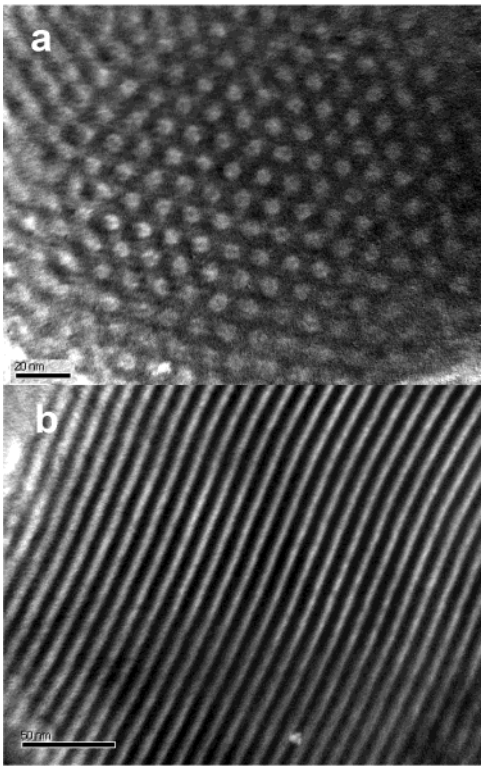

Figure 3. TEM images of sample MSE4 viewed (a) along the direction of the pore axis, and (b) along the direction perpendicular to the pore axis.

the ratios of (110)/(200) decrease with increasing acid concentrations despite a general weakness of the (110) reflections for samples ESE*y*. Taking the samples which were prepared with 24-h stirring for comparison purpose, the largest (110)/(200) ratio is seen on MSE2 and ESE3 samples for MSE*y* and ESE*y* materials, respectively.

The full width at half-maximum (fwhm) of an XRD peak can be used to evaluate the crystallinity of a crystalline phase:

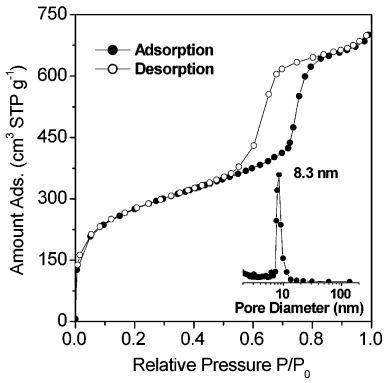

Figure 4. N_2 adsorption/desorption isotherm of MSE4. Inset: BJH pore size distribution of MSE4 determined from the adsorption isotherm.

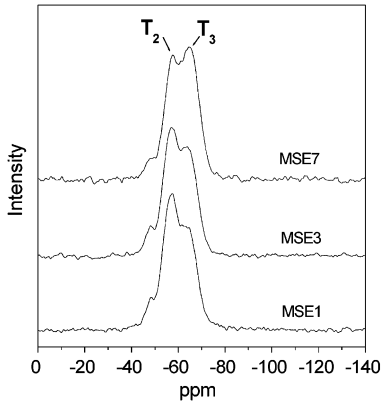

Figure 5. Solid-state ^{29}Si CP-MAS NMR spectra of representative MSE*y* materials.

the smaller the fwhm value, the greater the crystallinity and the larger the crystal size. For mesoscopically ordered materials with an amorphous framework, the fwhm of a SAXS peak can be used as an indication of the degree of structural ordering: the smaller the fwhm (i.e., the larger the fwhm^{-1}), the better the mesostructural ordering. Figure 2 depicts the reciprocal of fwhms of the (100) peaks as a function of HCl/H_2O molar ratio for the three types of mesoporous materials synthesized in this study. It is seen that for samples MSE*y*, fwhm^{-1} increases rapidly with decreasing HCl/H_2O molar ratio in the range of 2.25×10^{-2} to 7.08×10^{-4}, followed by a slightly decrease thereafter. For samples ESE*y*, the fwhm^{-1} values are generally lower than those of MSE*y* materials. Besides, materials ESE*y* are more sensitive to the changes of acid concentration than materials MSE*y*. In contrast to organosilica materials, no significant change of fwhm^{-1} with varying the HCl/H_2O molar ratios was observed on samples OS*y*.

The TEM images viewed along different directions of a representative sample, MSE4, are displayed in Figure 3. The well-ordered hexagonal arrays of mesopores and straight lattice fringes can be seen from the images viewed along and

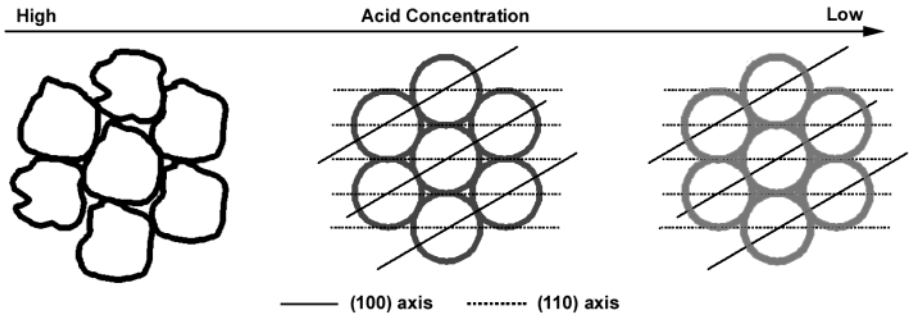

Figure 6. Schematic illustration of structural changes of PMO materials against acid concentration in the presence of P123. A darker color of the PMO framework indicates a higher degree of organosilicate condensation.

TABLE 3: Structural Parameters of MSE*y* Materials Determined from N_2 Adsorption Isotherms

sample	MSE1	MSE2	MSE3	MSE4	MSE5	MSE6	MSE7
D_{BJH} (nm)[a]	8.8	9.8	8.0	8.3	8.0	8.0	7.9
t (nm)[b]	4.1	3.1	4.6	4.5	4.4	4.8	4.7
S_{BET} (m^2/g)[c]	753	924	983	982	1011	969	930
V_{mes} (cm^3/g)[d]	0.54	0.72	0.72	0.74	0.63	0.58	0.23

[a] The pore sizes, D_{BJH}, were obtained from the peak positions of the BJH pore size distribution curves calculated from the adsorption branches of the isotherms. [b] Pore wall thicknesses, *t*, were calculated as a difference between the unit cell parameters, *a*, and the BJH pore sizes, D_{BJH}. [c] The specific surface areas, S_{BET}, were calculated by using the multiple-point Brunauer−Emmett−Teller (BET) method in the relative pressure range $P/P_0 = 0.05-0.26$. [d] The mesopore volumes, V_{mes}, were calculated by subtracting the microporous volumes, V_{mic}, from the primary pore volumes, V_p, according to the α_s-plot method.[29]

perpendicular to the pore axis, confirming the existence of a 2D hexagonal structure of a *p6mm* symmetry. TEM measurements of other high-quality samples gave similar images to that of sample MSE4.

A type IV isotherm with a H1 hysteresis loop, characteristic of mesoporous material with channel pores, is seen from the N_2 adsorption/desorption isotherms of the representative sample MSE4 (see Figure 4). The steep increase in N_2 volume adsorbed at $P/P_0 \approx 0.7$ indicates the uniformity of the mesopores in size, which was confirmed by the BJH pore size distribution curve (insert, Figure 4) with a narrow peak centered at about 8.3 nm. A summary of BJH pore size (D_{BJH}), pore wall thickness (t), BET specific surface area (S_{BET}), and primary mesopore volumes (V_{mes}) of the MSE*y* materials is reported in Table 3. A decrease in D_{BJH} with increasing amount of acid can be seen from Table 3, which is due to the contraction of the PPO cores of the P123 template.[30] It is also seen that V_{mes} increased steadily from sample MSE7 to MSE4, after which no obvious change is seen from MSE4 to MSE2, then decreased as the HCl/H_2O molar ratios were further lowered to 1.43×10^{-4}. Sample MSE4 possesses the largest mesopore volume, which is three-times higher than that of sample MSE7.

The solid-state ^{29}Si CP-MAS NMR spectra of three representative MSE*y* materials are displayed in Figure 5. Two prominent magnetic signals, which can be assigned to Si species covalently bonded to carbon atoms of T_2 [R′**Si**$(OH)(OSi)_2$] and T_3 [R′**Si**$(OSi)_3$],[20,24] are observed at −58 and −64 ppm, respectively. Decreasing acid content in the synthetic system resulted in a decreased degree of condensation as indicated by the decrease in the peak area ratio of T_3/T_2. Nevertheless, a significant level of condensation was still achieved for samples MSE1 and MSE3. The absence of Q_n [**Si**$(OSi)_n(OH)_{4-n}$] Si sites indicates that the Si−C bonds remained intact under our synthesis and subsequent treatment conditions. In agreement with the previous work,[24] one prominent signal corresponding to the ethylene carbons at about 4.7 ppm is seen from the solid-state ^{13}C CP-MAS NMR spectra of the three samples.

Discussion

As a catalyst in sol−gel synthetic chemistry, HCl acid accelerates the rates of hydrolysis and condensation of organosilica/silica precursors.[31] In the primary report of the synthesis of SBA-15 PMSs,[18] a large amount of acid ($HCl/H_2O = 2.83 \times 10^{-2}$) was used. It is thus unexpected that most previous studies on synthesizing SBA-15 PMOs adopted this synthesis strategy,[19−24] namely, a high acid concentration in synthesis gel. For examples, the HCl/H_2O ratios used in the previous studies were 3.83×10^{-2},[19] 3.59×10^{-2},[21] 2.91×10^{-2},[22] and 2.85×10^{-2},[24] respectively. However, according to our experimental data shown in Figure 2, none of the above acid concentrations falls in the region of the molar ratios of HCl/H_2O that favor the formation of a high-quality PMO mesostructure.

The silyl groups of the organosilica precursors BTMSE and BTESE are separated by ethylene bridge $-CH_2-CH_2-$. Therefore, in synthetic systems with identical silicon content, the organosilica systems possess less sites (hydroxyl groups or protonated hydroxyl groups) interacting with triblock copolymer P123 template in comparison with the pure-silica synthetic systems. Consequently, for the organosilica synthetic systems, the initial organosilicate-template assembly is relatively poorly organized compared with the PMS systems. In such a situation, slow condensation of the organosilicate is desired so that continuous rearrangement and reinforcement of the organosilica network at the organic and inorganic interfaces are occurring and the structural formation is more thermodynamically favored. However, BTMSE/BTESE hydrolyze and condense faster than TEOS due to the inductive effect of their ethylene bridges and the resulting increase in the density of the negative charges of the silicon and oxygen atoms.[31] To slow their condensation rates, a convenient way is to use a relatively low concentration of acid, which accelerates the rate of condensation of the organosilicates.[31]

The advantage of BTMSE in synthesizing structurally well-ordered PMOs over BTESE is because of its faster hydrolysis due to less steric hindrance resulting from the smaller methoxy unit,[31] as the hydrolyzed and oligomerized organosilica precursors are primarily responsible for interactions with the triblock copolymer.[32]

The prolonged precipitation time with decreasing HCl/H_2O ratios for the three systems investigated in this study is a result of the acceleration effect of the acid for the hydrolysis and condensation of the organosilica/silica precursors. At high acid concentrations, the precipitation time of the three systems follows the sequence of TEOS > BTESE > BTMSE. While the faster precipitation of the BTMSE system than that of

BTESE system is due to less steric hindrance because of smaller methoxy units, the faster precipitation of BTSEM and BTESE systems than that of TEOS system at high HCl/H_2O ratios is mainly due to the inductive effect of ethylene bridges. Seemingly contrary to what is predicted by the inductive effect, at extremely low acid concentrations, the precipitation time of samples OS1 and OS2 were less than 24 h, whereas no precipitation was observed for samples MSE1, ESE1, and ESE2 within 24 h under the low acid concentrations. The above facts suggest that in a combination of sol−gel and self-assembly processes, the comparison of the relative rates of hydrolysis and condensation between organosilica and silica precursors is more complex than those of a pure sol−gel process. The cooperative assembly process of the hydrolyzed organosilica/silica precursors with the template is known to be favorable for intermolecular condensation due to an enrichment of the local organosilica/silica oligomers concentration.[33,34] The faster precipitation of TEOS system at extremely low acid concentrations is another support of the stronger interactions between hydrolyzed TEOS and the template as described above.

Although some authors[28,35,36] correlated the increase in the peak intensity ratios of (110)/(200) to a decrease in pore wall thickness, the increase of the (110)/(200) peak intensity ratio is more commonly attributed to an increase in the density of scatterers along the (110) axis due to an increasing condensed silica framework.[37−40] For the OSy materials, the observed increase in the peak intensity ratios of (110)/(200) with increasing acid concentrations in the initial synthesis gels is most probably due to the increasingly condensed silicate frameworks as acid is known to accelerate and promote the degree of silicate condensation.[31,39,40] However, from our experimental data, it seems that for SBA-15 PMOs, the increase in the density of scatterers along the (110) axis occurred only when the acid concentration in the synthetic system was lowered. As shown by the ^{29}Si CP-MAS NMR spectra in Figure 5, a decreased level of condensation is observed as the acid content was lowered in the synthetic gels. This unusual behavior of SBA-15 PMOs is believed to be related to the condensation properties of their synthetic precursors. In their studies on hexagonally ordered zirconia and silica, Schüth and co-workers[37,38] proposed that at the initial stage of the self-assembly process, the hexagonal mesophase is made up of close-packed rodlike inorganic-surfactant composite aggregates which behave similarly to normal surfactant aggregates. An increase in the degree of condensation enhances the inorganic−inorganic contact, which in turn increases the amount of good scatterers along the (110) axis without changing significantly the scatterer density in the (100) and (200) axis.[37,38] However, in the case of organosilica precursors, which interact poorly with surfactant and condense faster than zirconia and silica precursors, a high acid concentration such as that used for synthesizing MSE7 would lead to a rapid condensation of the organosilica precursors around the close-packed rodlike micelle aggregates, resulting in small hexagonal domains with poorly defined pores as schematically illustrated in Figure 6. Decreasing the amount of acid decreased the rate of condensation, allowing further refining of the pore shape as well as an increase in the size of the hexagonal domains. However, because the rate of condensation is still relatively high, the maximization of organosilica−organosilica contact within the close-packed rodlike organosilica−surfactant composite aggregates is kinetically hindered due to the preformed, highly condensed organosilica framework, resulting in the deficiency of the good scatterers in the (110) axis (see Figure 6). Further decrease in acid concentration slows down the rate of condensation even more, making the maximization of the organosilica−organosilica contact feasible, which enhances the density of the good scatterers along the (110) axis despite an overall decrease in the level of framework condensation.

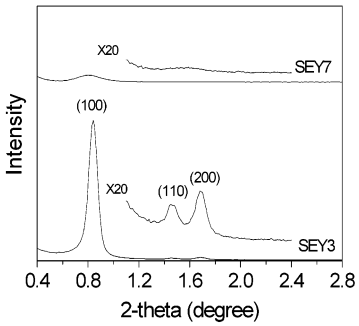

Figure 7. SAXS patterns of ethenylene-bridged PMOs synthesized with HCl/H_2O ratios of 2.25×10^{-2} (SEY7) and 7.08×10^{-4} (SEY3).

Conclusions

In conclusion, we have, for the first time, identified the critical role of acid in the synthesis of high-quality large-pore ethylene-bridged PMOs. Unlike large-pore PMSs which can be synthesized over a wide range of acid concentrations, highly ordered, ethylene-bridged, large-pore PMOs can only be synthesized under controlled low acid concentrations. Under the synthesis conditions described in this work, BTMSE was found to be a better organosilica source than BTESE. The organo-spacer R′ and its effect on the hydrolysis and condensation behaviors of the organosilica precursors were identified to play a critical role in the self-assembly of surfactant−organosilica composites, thus resulting in an unusual synthetic strategy for high-quality PMOs. In addition, such a low-acid-concentration synthetic strategy has been found to be equally workable for other PMO materials such as ethenylene-bridged (where $R' = -CH_2{=}CH_2-$) PMOs.

Acknowledgment. This work was financially supported by ARF of NUS and A*STAR. X.Y.B. thanks NUS for offering a scholarship.

References and Notes

(1) Inagaki, S.; Guan, S.; Fukushima, Y.; Ohsuna, T.; Terasaki, O. *J. Am. Chem. Soc.* **1999**, *121*, 9611.
(2) Melde, B. J.; Holland, B. T.; Blanford, C. F.; Stein, A. *Chem. Mater.* **1999**, *11*, 3302.
(3) Asefa, T.; MacLachlan, M. J.; Coombs, N.; Ozin, G. A. *Nature* **1999**, *402*, 867.
(4) Lu, Y.; Fan, H.; Doke, N.; Loy, D. A.; Assink, R. A.; LaVan, D. A.; Brinker, C. J. *J. Am. Chem. Soc.* **2000**, *122*, 5258.
(5) Inagaki, S.; Guan, S.; Ohsuna, T.; Terasaki, O. *Nature* **2002**, *416*, 304.
(6) Kuroki, M.; Asefa, T.; Whitnal, W.; Kruk, M.; Yoshina-Ishii, C.; Jaroniec, M.; Ozin, G. A. *J. Am. Chem. Soc.* **2002**, *124*, 13886.
(7) Dag, O.; Yoshina-Ishii, C.; Asefa, T.; MacLachlan, M. J.; Grondey, H.; Coombs, N.; Ozin, G. A. *Adv. Funct. Mater.* **2001**, *11*, 213.
(8) MacLachlan, M. J.; Asefa, T.; Ozin, G. A. *Chem.−Eur. J.* **2000**, *6*, 2507.
(9) Stein, A.; Melde, B. J.; Schroden, R. K. *Adv. Mater.* **2000**, *12*, 1403.
(10) Sayari, A.; Hamoudi, S. *Chem. Mater.* **2001**, *13*, 3151.
(11) Wight, A. P.; Davis, M. E. *Chem. Rev.* **2002**, *102*, 3589.
(12) Sanchez, C.; Soler-Illia, G. J. D. A.; Ribot, F.; Lalot, T.; Mayer, C. R.; Cabuil, V. *Chem. Mater.* **2001**, *13*, 3061.
(13) Loy, D. A.; Shea, K. J. *Chem. Rev.* **1995**, *95*, 1431.
(14) Baleizão, C.; Gigante, B.; Das, D.; Alvaro, M.; Garcia, H.; Corma, A. *Chem. Commun.* **2003**, 1860.
(15) Burleigh, M. C.; Markowitz, M. A.; Spector, M. S.; Gaber, B. P. *Environ. Sci. Technol.* **2002**, *36*, 2515.
(16) Fukuoka, A.; Sakamoto, Y.; Guan, S.; Inagaki, S.; Sugimoto, N.; Fukushima, Y.; Hirahara, K.; Iijima, S.; Ichikawa, M. *J. Am. Chem. Soc.* **2001**, *123*, 3373.

(17) Beck, J. S.; Vartuli, C.; Roth, W. J.; Leonowicz, M. E.; Kresge, C. T.; Schmitt, K. D.; Chu, T.-W.; Olson, D. H.; Sheppard, E. W.; McCullen, S. B.; Higgins, J. B.; Schlenker, J. L. *J. Am. Chem. Soc.* **1992**, *114*, 10834.

(18) Zhao, D.; Huo, Q.; Feng, J.; Chmelka, B. F.; Stucky, G. D. *J. Am. Chem. Soc.* **1998**, *120*, 6024.

(19) Burleigh, M. C.; Markowitz, M. A.; Wong, E. M.; Lin, J. S.; Gaber, G. P. *Chem. Mater.* **2001**, *13*, 4411.

(20) Cho, E. B.; Kwon, K. W.; Char, K. *Chem. Mater.* **2001**, *13*, 3837.

(21) Muth, O.; Schellbach, C.; Fröba, M. *Chem. Commun.* **2001**, 2032.

(22) Matos, J. R.; Kruk, M.; Mercuri, L. P.; Jaroniec, M.; Asefa, T.; Coombs, N.; Ozin, G. A.; Kamiyama, T.; Terasaki, O. *Chem. Mater.* **2002**, *14*, 1903.

(23) Zhu, H. G.; Jones, D. J.; Zajac, J.; Roziere, J.; Dutartre, R. *Chem. Commun.* **2001**, 2568.

(24) Guo, W. P.; Park, J. Y.; Oh, M. O.; Jeong, H. W.; Cho, W. J.; Kim, I.; Ha, C. S. *Chem. Mater.* **2003**, *15*, 2295.

(25) Pauly, T. R.; Petkov, V.; Liu, Y.; Billinge, S. J. L.; Pinnavaia, T. J. *J. Am. Chem. Soc.* **2002**, *124*, 97.

(26) Soler-Illia, G. J. D. A.; Crepaldi, E. L.; Grosso, D.; Sanchez, C. *Curr. Opin. Colloid Interface Sci.* **2003**, *8*, 109.

(27) Kleitz, F.; Choi, S. H.; Ryoo, R. *Chem. Commun.* **2003**, 2136.

(28) Kruk, M.; Jaroniec, M.; Ko, C. H.; Ryoo, R. *Chem. Mater.* **2000**, *12*, 1961.

(29) Gregg, S. J.; Sing, K. S. W. *Adsorption, Surface Area and Porosity*; Academic Press: London, 1982.

(30) Schmidt-Winkel, P.; Yang, P. D.; Margolese, D. I.; Chmelka, B. F.; Stucky, G. D. *Adv. Mater.* **1999**, *11*, 303.

(31) Brinker, C. J. *J. Non-Cryst. Solids* **1988**, 100, 31.

(32) Kim, J. M.; Han, Y. J.; Chmelka, B. F.; Stucky, G. D. *Chem. Commun.* **2000**, 2437.

(33) Monnier, A.; Schüth, F.; Huo, Q.; Kumar, D.; Margolese, D.; Maxwell, R. S.; Stucky, G. D.; Krishnamurty, M.; Petroff, P.; Firouzi, A.; Janicke, M.; Chmelka, B. F. *Science* **1993**, *261*, 1299.

(34) Firouzi, A.; Kumar, D.; Bull, L. M.; Besier, T.; Sieger, P.; Huo, Q.; Walker, S. A.; Zasadzinski, J. A.; Glinka, C.; Nicol, J.; Margolese, D.; Stucky, G. D.; Chmelka, B. F. *Science* **1995**, *267*, 1138.

(35) Feuston, B. P.; Higgins, J. B. *J. Phys. Chem. B* **1994**, *98*, 4459.

(36) Kruk, M.; Jaroniec, M.; Sayari, A. *Chem. Mater.* **1999**, *11*, 492.

(37) Linden, M.; Blanchard, J.; Schacht, S.; Schunk, S. A.; Schüth, F. *Chem. Mater.* **1999**, *11*, 3002.

(38) Agren, P.; Linden, M.; Rosenholm, J. B.; Schwarzenbacher, R.; Kriechbaum, M.; Amenitsch, H.; Laggner, P.; Blanchard, J.; Schüth, F. *J. Phys. Chem. B.* **1999**, *103*, 5943.

(39) Impéror-Clerc, M.; Davidson, P.; Davidson, A. *J. Am. Chem. Soc.* **2000**, *122*, 11925.

(40) Gross, A. F.; Le, V. H.; Kirsch, B. L.; Riley, A. E.; Tolbert, S. H. *Chem. Mater.* **2001**, *13*, 3571.